Supplementary Information

for

"Retrieving Vortex-Driven Non-Hermiticity from Trajectory-Resolved Measurements in Optical Levitation"

Mian Wu[1]†, Xiao Li[2]†, Nan Li[1]†, Han Cai[1]*, Jack Ng[3]*, C. T. Chan[2], and Huizhu Hu[1]*

[1]College of Optical Science and Engineering, and State Key Laboratory for Extreme Photonics and Instrumentation, Zhejiang University, Hangzhou, 310027, Zhejiang, China

[2]Department of Physics and State Key Laboratory of Optical Quantum Materials, The Hong Kong University of Science and Technology, Clear Water Bay, Hong Kong SAR, China

[3]State Key Laboratory of Quantum Functional Materials, Department of Physics, and Guangdong Basic Research Center of Excellence for Quantum Science, Southern University of Science and Technology (SUSTech), Shenzhen, 518055, Guangdong, China

*Corresponding author(s). E-mail(s): hancai@zju.edu.cn; wuzh3@sustech.edu.cn; huhuizhu2000@zju.edu.cn;

†These authors contributed equally to this work.

Supplementary Note 1: General theory for the stability analysis of optically trapped or optically bound particles.

Intense laser fields confine small particles near intensity extrema, a phenomenon known as optical trapping. In addition, light scattered by multiple particles modifies the spatial field distribution and mediates particle-particle interactions known as optical binding. Optical trapping and binding can drive particles towards an equilibrium at which the net force vanishes. The existence of an equilibrium, however, does not guarantee stability: following a perturbation, particles either return to the equilibrium or move away from it. A rigorous stability analysis is therefore required and is presented below.

Particles illuminated by light and immersed in a fluid experience optical forces, dissipative ambient damping, hydrodynamic couplings [i], and Brownian fluctuations. To obtain analytical solutions in this Supplementary Note, we consider well-separated microparticles illuminated by a laser field of modest intensity (for example, I_0 = 1.0 mW/μm^2), for which hydrodynamic coupling can be neglected. Because the eigenmodes are independent of the excitation, they are unaffected by Brownian motion.

For a cluster of N particles in a fluid, the equation of motion, neglecting hydrodynamic coupling and Brownian motion, is [ii]

$$m\frac{d^2\mathbf{r}}{dt^2} = \mathbf{F}(\mathbf{r}) - \gamma\frac{d\mathbf{r}}{dt}, \tag{S1}$$

where m is the mass of each particle and t is time. The friction coefficient is [iii]

$$\gamma = 6\pi\eta r_{\mathrm{S}}\frac{0.619}{0.619+\mathrm{Kn}}(1+c_{\mathrm{K}}), \tag{S2}$$

Here, η is the viscosity of air, r_{S} is the particle radius, $\mathrm{Kn} = \dfrac{\lambda_{\mathrm{mfp}}}{r_{\mathrm{S}}}$ is the Knudsen number, $\lambda_{\mathrm{mfp}} = \lambda_{\mathrm{mfp}}^{\mathrm{Air}}\dfrac{P_{\mathrm{atm}}}{P}$ is the mean free path in a background medium at pressure P, P_{atm} is standard atmospheric pressure, $\lambda_{\mathrm{mfp}}^{\mathrm{Air}} = 68$ nm is the mean free path in air, and $c_{\mathrm{K}} = \dfrac{0.31\mathrm{Kn}}{0.785+1.152\mathrm{Kn}+\mathrm{Kn}^2}$.

The vectors $\mathbf{F}(\mathbf{r}) = \left(F_{x,1}, F_{y,1}, F_{z,1}, \cdots, F_{x,N}, F_{y,N}, F_{z,N}\right)$ and $\mathbf{r} = \left(x_1, y_1, z_1, \cdots, x_N, y_N, z_N\right)$ denote, respectively, the optical forces on the N particles and their displacements from the equilibrium position $\mathbf{r}_0 = \left(x_{0,1}, y_{0,1}, z_{0,1}, \cdots, x_{0,N}, y_{0,N}, z_{0,N}\right)$, where $\mathbf{F}(\mathbf{r}_0) = \mathbf{0}$. For simplicity, we set $\mathbf{r}_0 = \mathbf{0}$. The stability of Eq. (S1) near an equilibrium is equivalent to that of its linearization [iv]:

$$m\frac{d^2\mathbf{r}}{dt^2} = \ddot{\mathbf{K}} \cdot \mathbf{r} - \gamma\frac{d\mathbf{r}}{dt}, \tag{S3}$$

where $\ddot{\mathbf{K}}_{ij} = \partial \mathbf{F}_i / \partial \mathbf{r}_j$ is the force constant matrix and $\ddot{\mathbf{K}} \cdot \mathbf{r}$ is the linear approximation to $\mathbf{F}(\mathbf{r})$.

Away from an exceptional point (EP), at which $\ddot{\mathbf{K}}$ is defective, Eq. (S3) can be diagonalized through a similarity transformation by $\ddot{\mathbf{V}}$, whose columns are the normalized right eigenvectors of $\ddot{\mathbf{K}}$. Equation (S3) then reduces to a set of decoupled second-order differential equations:

$$m\frac{d^2\zeta_i}{dt^2} \approx K_i \cdot \zeta_i - \gamma\frac{d\zeta_i}{dt}, \tag{S4}$$

where K_i is the i^{th} eigenvalue of $\ddot{\mathbf{K}}$, that is, $\left(\ddot{\Lambda}\right)_{ij} = \left(\ddot{\mathbf{V}}^{-1}\ddot{\mathbf{K}}\ddot{\mathbf{V}}\right)_{ij} = K_i\delta_{i,j}$, and $\zeta = \ddot{\mathbf{V}}^{-1}\mathbf{r}$. Here, $\delta_{i,j}$ is the Kronecker delta. Equation (S4) can be solved using the standard substitution technique:

$$\zeta_i = \zeta_{0,i}e^{-i\Omega_i t}, \tag{S5}$$

where ζ_0 is a time-independent scalar to be determined by initial conditions. The solutions of Eq. (S4) can be classified according to K_i, or equivalently according to the natural frequency of the eigenmode, defined by

$$\Omega_i = \Omega_{i,0} = \sqrt{-K_i / m}. \tag{S6}$$

Including background damping, the vibrational frequencies of the i^{th} mode (K_i) are

$$\Omega_i^{\pm} = -\frac{i\gamma}{2m} \pm \sqrt{-\frac{K_i}{m} - \left(\frac{\gamma}{2m}\right)^2}. \tag{S7}$$

We next distinguish several stability regimes according to the nature of K_i.

a) Unstable mode: positive K_i (imaginary $\Omega_{i,0}$).

For $K_i > 0$, $\Omega_{i,0}$ is purely imaginary, and the corresponding eigenmode is

$$\mathbf{r}_i(t) = e^{-\gamma t/2m}\mathbf{V}_i \times \left[\alpha_i e^{+t\sqrt{(\gamma/2m)^2+|\Omega_{i,0}|^2}} + \beta_i e^{-t\sqrt{(\gamma/2m)^2+|\Omega_{i,0}|^2}} \right], \tag{S8}$$

where $\mathbf{V}_i$ is the i^{th} eigenvector of K_i, and α_i and β_i are constants determined by the initial conditions. Equation (S8) diverges with time; the mode is therefore unstable.

b) Stable mode: negative K_i (real $\Omega_{i,0}$).

For $K_i < 0$, the modes are harmonic-oscillation-like:

$$\mathbf{r}_i(t) = \begin{cases} e^{-\gamma t/2m}\mathbf{V}_i \times \left[\alpha_i e^{+t\sqrt{(\gamma/2m)^2-\Omega_{i,0}{}^2}} + \beta_i e^{-t\sqrt{(\gamma/2m)^2-\Omega_{i,0}{}^2}} \right] & \text{if } (\gamma/2m)^2 > \Omega_{i,0}{}^2 \text{ (overdamped)} \\ e^{-\gamma t/2m}\mathbf{V}_i \times \left[\alpha_i + \beta_i t \right] & \text{if } (\gamma/2m)^2 = \Omega_{i,0}{}^2 \text{ (critically damped),} \\ A_i e^{-\gamma t/2m}\mathbf{V}_i \times \sin\left[\sqrt{\Omega_{i,0}{}^2 - (\gamma/2m)^2}\, t + \varphi_i \right] & \text{if } (\gamma/2m)^2 < \Omega_{i,0}{}^2 \text{ (underdamped)} \end{cases} \tag{S9}$$

where α_i and β_i, or A_i and φ_i, are constants determined by the initial conditions. All these modes are stable.

c) Complex mode: complex K_i (complex $\Omega_{i,0}$).

Optically trapped or bound particles form an open system, and the optical forces acting on them are generally nonconservative. Consequently, $\ddot{\mathbf{K}} \neq \ddot{\mathbf{K}}^{\dagger}$, or equivalently $\ddot{\mathbf{K}} \neq \ddot{\mathbf{K}}^{T}$ for real $\ddot{\mathbf{K}}$. Complex-conjugate pairs of eigenvalues are therefore permitted even when $\ddot{\mathbf{K}}$ is real. The modes associated with the conjugate pair are

$$\begin{aligned} \mathbf{r}_{i+}(t) &= \alpha_i e^{-\mathrm{Im}(\Omega_{i+})t} \times \left\{ \mathrm{Re}[\mathbf{V}_i]\cos\left(\mathrm{Re}[\Omega_{i+}]t + \varphi_{i\alpha}\right) - \mathrm{Im}[\mathbf{V}_i]\sin\left(\mathrm{Re}[\Omega_{i+}]t + \varphi_{i\alpha}\right) \right\}, \\ \mathbf{r}_{i-}(t) &= \beta_i e^{-\mathrm{Im}(\Omega_{i-})t} \times \left\{ \mathrm{Re}[\mathbf{V}_i]\cos\left(\mathrm{Re}[\Omega_{i-}]t + \varphi_{i\beta}\right) + \mathrm{Im}[\mathbf{V}_i]\sin\left(\mathrm{Re}[\Omega_{i-}]t + \varphi_{i\beta}\right) \right\}, \end{aligned} \tag{S10}$$

where α_i, β_i, $\varphi_{i\alpha}$, and $\varphi_{i\beta}$ are constants determined by the initial conditions,

$$\begin{aligned}\mathrm{Re}(\Omega_{i\pm}) &= \mp\left[(\gamma^2+4m\,\mathrm{Re}[K_i])^2+16m^2\,\mathrm{Im}[K_i]^2\right]^{1/4}\sin(\delta_i/2)/2m,\\ \mathrm{Im}(\Omega_{i\pm}) &= \gamma \pm\left[(\gamma^2+4m\,\mathrm{Re}[K_i])^2+16m^2\,\mathrm{Im}[K_i]^2\right]^{1/4}\cos(\delta_i/2)/2m,\end{aligned} \tag{S11}$$

and

$$\delta_i = \begin{cases} \tan^{-1}\dfrac{4m\left|\mathrm{Im}[K_i]\right|}{\gamma^2+4m\,\mathrm{Re}[K_i]} & \text{if} \quad \gamma^2+4m\,\mathrm{Re}[K_i]>0,\\ \pi-\tan^{-1}\dfrac{4m\left|\mathrm{Im}[K_i]\right|}{\left|\gamma^2+4m\,\mathrm{Re}[K_i]\right|} & \text{if} \quad \gamma^2+4m\,\mathrm{Re}[K_i]<0. \end{cases} \tag{S12}$$

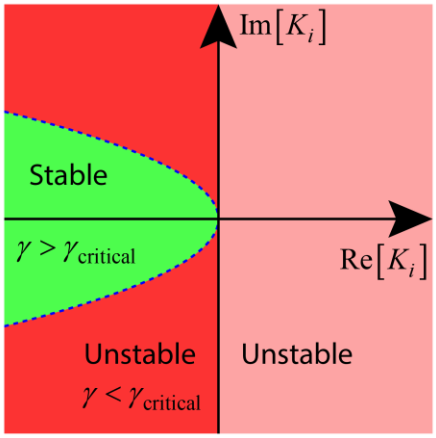

Fig. S1 | Stability as a function of K_i. The stable region is shown in green ($\gamma > \gamma_{\mathrm{critical}}$); unstable regions are shown in red ($\gamma < \gamma_{\mathrm{critical}}$) and pink ($\mathrm{Re}[K_i]>0$). The blue dashed line denotes $\gamma = \gamma_{\mathrm{critical}}$.

The stability regimes of the complex modes are summarized in Fig. S1. For $\mathrm{Re}[K_i]>0$ (pink region in Fig. S1), both conservative and nonconservative forces induce instability. The conservative contribution corresponds to a potential-energy maximum, whereas the nonconservative contribution produces a centrifugal force that drives the particles away from equilibrium. The cluster is therefore unstable. For $\mathrm{Re}[K_i]<0$ and

$\gamma < \gamma_{\text{critical}} = \sqrt{m}\left|\text{Im}[K_i]\right| / \sqrt{\left|\text{Re}[K_i]\right|}$ (red region in Fig. S1), the conservative force attracts the particles towards equilibrium, but the nonconservative force drives circulation at increasing speed and ultimately overcomes this attraction and thus the configuration is unstable. By contrast, if $\text{Re}[K_i] < 0$ and $\gamma > \gamma_{\text{critical}}$ (green region in Fig. S1), damping removes the kinetic energy injected by the nonconservative force field sufficiently rapidly to stabilize the cluster.

d) Stability at exceptional points (EPs)

For completeness, we analyze the stability of a system at an exceptional point (EP), where the particles are subject to optical forces and ambient damping. Without loss of generality, we consider an arbitrary 2×2 force constant matrix; a comprehensive treatment of matrices of arbitrary size is given in Ref. [**Error! Bookmark not defined.**]. After an appropriate rotation, a general force constant matrix can be written as

$$\ddot{\mathbf{K}} = \begin{bmatrix} a+b & -g \\ g & a-b \end{bmatrix}, \tag{S13}$$

where $b = g$ defines the EP, at which $\ddot{\mathbf{K}}$ becomes defective and has only one linearly independent eigenvector,

$$\mathbf{V}_1 = \begin{bmatrix} -1 \\ 1 \end{bmatrix}, \tag{S14}$$

satisfying

$$\ddot{\mathbf{K}}\mathbf{V}_1 = a\mathbf{V}_1. \tag{S15}$$

To characterize the Jordan structure of the force constant matrix, we introduce the generalized eigenvector $\mathbf{U}_1$, defined by

$$\left(\ddot{\mathbf{K}} - a\ddot{\mathbf{I}}\right)\mathbf{U}_1 = \mathbf{V}_1, \tag{S16}$$

from which

$$\mathbf{U}_1 = \begin{bmatrix} -1/g \\ 0 \end{bmatrix} \tag{S17}$$

This generalized eigenvector is specific to the defective force constant matrix and establishes its Jordan canonical form.

To investigate stability in the presence of viscous damping $-\gamma \frac{d\mathbf{r}}{dt}$, we next consider the equation of motion in Eq. (S3).

The eigenfrequencies are given by Eq. (S7):

$$\Omega_{\mathrm{EP}}^{\pm} = -\frac{i\gamma}{2m} \pm \sqrt{-\frac{a}{m} - \left(\frac{\gamma}{2m}\right)^2}\,, \tag{S18}$$

where a is the eigenvalue K_i of $\vec{\vec{\mathbf{K}}} = \begin{bmatrix} a+g & -g \\ g & a-g \end{bmatrix}$ at the EP. Assuming a harmonic solution ($\mathbf{r}(t) = \mathbf{X}e^{-i\Omega_i t}$), the equation of motion reduces to the quadratic eigenvalue problem:

$$\vec{\vec{\mathbf{P}}}(\Omega_i)\mathbf{X} = \left(m\Omega_i^2 \vec{\vec{\mathbf{I}}} + i\gamma\Omega_i \vec{\vec{\mathbf{I}}} + \vec{\vec{\mathbf{K}}}\right)\mathbf{X} = 0\,. \tag{S19}$$

At the exceptional point, the eigenvalue $\Omega_i = \Omega_{\mathrm{EP}}^{\pm}$ is defective and only one eigenvector exists. The conventional modal expansion is therefore incomplete, and the second linearly independent solution must be constructed using a generalized eigenvector [v]. The generalized eigenvector of the quadratic eigenvalue problem satisfies

$$\vec{\vec{\mathbf{P}}}(\Omega_i)\mathbf{U} = -\frac{d\vec{\vec{\mathbf{P}}}(\Omega_i)}{d\Omega_i}\mathbf{V}\,, \tag{S20}$$

where

$$\frac{d\vec{\vec{\mathbf{P}}}(\Omega_i)}{d\Omega_i} = \frac{d}{d\Omega_i}\left(m\Omega_i^2 \vec{\vec{\mathbf{I}}} + i\gamma\Omega_i \vec{\vec{\mathbf{I}}} + \vec{\vec{\mathbf{K}}}\right) = \left(2m\Omega_i + i\gamma\right)\vec{\vec{\mathbf{I}}}\,. \tag{S21}$$

Because $\frac{d\vec{\vec{\mathbf{P}}}(\Omega_i)}{d\Omega_i}$ is proportional to the identity matrix $\vec{\vec{\mathbf{I}}}$,

$$\vec{\vec{\mathbf{P}}}(\Omega_i)\mathbf{U} = -\left(2m\Omega_i + i\gamma\right)\mathbf{V}\,. \tag{S22}$$

The two independent solutions at the exceptional point ($\Omega_i = \Omega_{\mathrm{EP}}^{\pm}$) are therefore [vi]

$$\mathbf{r}_1 = \alpha_1 \mathbf{V}_1 e^{-i\Omega_{\mathrm{EP}}^{\pm} t} = \alpha_1 \mathbf{V}_1 e^{-\frac{\gamma}{2m}t} e^{\mp i\sqrt{-\frac{a}{m}-\left(\frac{\gamma}{2m}\right)^2}\,t}. \tag{S23}$$

and

$$\mathbf{r}_2 = \alpha_2 \left[\mathbf{U}_1 - i\left(2m\Omega_{\mathrm{EP}}^{\pm} + i\gamma\right)t\mathbf{V}_1 \right] \mathbf{V}_1 e^{-i\Omega_{\mathrm{EP}}^{\pm} t} = \alpha_2 \left[\mathbf{U}_1 - i\left(2m\Omega_{\mathrm{EP}}^{\pm} + i\gamma\right)t\mathbf{V}_1 \right] e^{-\frac{\gamma}{2m}t} e^{\mp i\sqrt{-\frac{a}{m}-\left(\frac{\gamma}{2m}\right)^2}\,t}, \tag{S24}$$

where α_1 and α_2 are constants determined by the initial conditions. The second solution contains a factor linear in time, a direct consequence of the Jordan-block structure of the force constant matrix. Whereas each ordinary eigenmode evolves independently as a pure exponential, eigenvector coalescence at the EP introduces the additional polynomial factor t that is characteristic of defective eigenvalue problems.

As in Eq. (S9), the overdamped, critically damped, and underdamped cases all decay in time, implying that any ambient damping stabilizes the particles at an exceptional point of the force constant matrix, provided that $a < 0$.

Supplementary Note 2: Non-Hermitian theory for the optical trapping of a single spherical particle.

a) Derivation of the 2×2 force constant matrix for transverse motion

We consider a single spherical particle trapped by a tightly focused Gaussian beam of arbitrary polarization. The general force constant matrix $\ddot{\mathbf{K}}_{ij} = \partial \mathbf{F}_i / \partial \mathbf{r}_j$ for a single particle is

$$\ddot{\mathbf{K}}_{3\times3} = \begin{bmatrix} k_{xx} & k_{xy} & k_{xz} \\ k_{yx} & k_{yy} & k_{yz} \\ k_{zx} & k_{zy} & k_{zz} \end{bmatrix}. \tag{S25}$$

For the time-averaged optical force, the trapping system is invariant under a 180° rotation about the z axis, which reverses the x and y components of both the force and displacement vectors. Under this rotation, $k_{xz} = \dfrac{\partial F_x}{\partial z}$ transforms into $k_{xz} = \dfrac{\partial \left(-F_x\right)}{\partial z}$, implying that $k_{xz} = 0$. Similarly, $\ddot{\mathbf{K}}_{3\times3}$ can be reduced to

$$\ddot{\mathbf{K}}_{3\times3} = \begin{bmatrix} k_{xx} & k_{xy} & 0 \\ k_{yx} & k_{yy} & 0 \\ 0 & 0 & k_{zz} \end{bmatrix}. \tag{S26}$$

The z motion is therefore decoupled from, and independent of, the x and y motion. We focus on transverse motion because the z motion is simple harmonic and its physics is well established. The most general form of the remaining 2×2 transverse force constant matrix is

$$\ddot{\mathbf{K}}'_{2\mathrm{D}} = \begin{bmatrix} a'+b' & d'-g' \\ d'+g' & a'-b' \end{bmatrix}, \tag{S27}$$

where all components are real, and d' and g' are the Hermitian (symmetric) and non-Hermitian (antisymmetric) coupling components, respectively. The non-Hermitian character of this matrix places the system within the broader framework of non-Hermitian physics. A rotation can always eliminate the symmetric coupling. Without loss of generality, the force constant matrix can therefore be rewritten as

$$\ddot{\mathbf{K}}_{2D} = \begin{bmatrix} a+b & -g \\ g & a-b \end{bmatrix}, \tag{S28}$$

where a nonzero g quantifies the non-Hermiticity and enforces $\ddot{\mathbf{K}}_{2D} \neq \ddot{\mathbf{K}}_{2D}^{\dagger}$.

b) Inevitable emergence of non-Hermiticity and an exceptional point as the polarization changes from linear to circular

The matrix $\ddot{\mathbf{K}}_{2D}$ is non-Hermitian if and only if the incident beam carries orbital angular momentum [vii]. Here, this orbital angular momentum arises from the conversion of spin angular momentum during focusing [viii]. The eigenvalues of $\ddot{\mathbf{K}}_{2D}$ are

$$K_{\pm} = a \pm \sqrt{b^2 - g^2}\,, \tag{S29}$$

where $b = g$ defines an exceptional point at which the two eigenvalues and eigenvectors coalesce.

We vary the incident polarization continuously from linear (Fig. S2a), through elliptical, to circular (Fig. S2b), as parameterized by

$$\hat{\mathbf{p}} = \hat{\mathbf{x}}\cos\theta + i\hat{\mathbf{y}}\sin\theta\,, \tag{S30}$$

Here, $\theta = 0°$ and $\theta = 45°$ correspond to linear and circular polarization, respectively. For linear polarization, the light illuminating the objective carries no net spin angular momentum; symmetry therefore forbids the generation of net orbital angular momentum upon focusing, so $g = 0$. Nevertheless, the transverse field pattern is anisotropic [ix] (Fig. S2c), yielding a nonzero b. For circular polarization, the field pattern is circularly symmetric (Fig. S2d) [ix], so $b = 0$, whereas spin-to-orbital angular-momentum conversion produces a nonzero g. As the polarization changes continuously from linear ($\theta = 0°$) to circular ($\theta = 45°$), b decreases to zero while g increases from zero. The two quantities must therefore intersect, as illustrated in Fig. S3, and this intersection is the exceptional point.

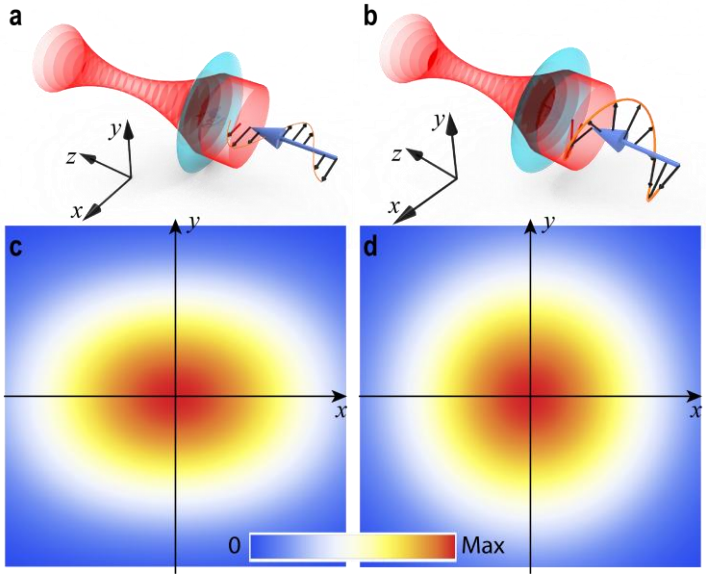

Fig. S2 | Light-intensity distributions for focused beams of different polarizations. (a) Intensity in the *xy* plane for linear polarization. (b) Intensity in the *xy* plane for circular polarization.

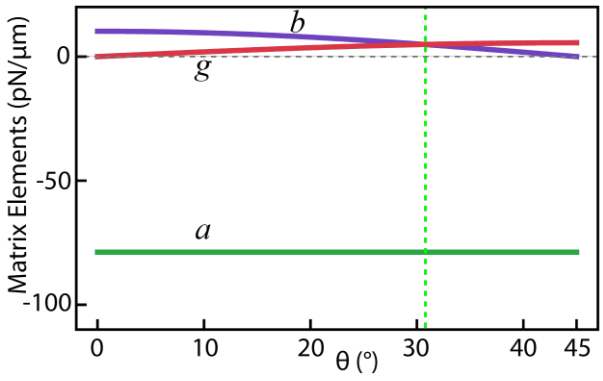

Fig. S3 | Components of $\ddot{\mathbf{K}}_{2D} = \begin{bmatrix} a+b & -g \\ g & a-b \end{bmatrix}$ as the incident polarization varies from linear ($\theta = 0°$) to circular ($\theta = 45°$).

Supplementary Note 3: Non-Hermitian optical binding of three spherical particles.

We theoretically and experimentally investigate the non-Hermitian optical binding of three silica particles in vacuum. Each particle is levitated by a focused, linearly polarized beam, and the particles form a triangle in the transverse plane (Fig. S4a). The base of the triangle is approximately 3.45 μm, a geometry chosen to enhance the non-Hermitian couplings while suppressing the Hermitian couplings (Fig. S4b).

a) Decoupling of longitudinal and transverse motion

For three particles, the general force constant matrix takes the form

$$\ddot{\mathbf{K}}_{9\times 9} = \begin{bmatrix} k_{xx}^{1-1} & k_{xy}^{1-1} & k_{xz}^{1-1} & k_{xx}^{1-2} & k_{xy}^{1-2} & k_{xz}^{1-2} & k_{xx}^{1-3} & k_{xy}^{1-3} & k_{xz}^{1-3} \\ k_{yx}^{1-1} & k_{yy}^{1-1} & k_{yz}^{1-1} & k_{yx}^{1-2} & k_{yy}^{1-2} & k_{yz}^{1-2} & k_{yx}^{1-3} & k_{yy}^{1-3} & k_{yz}^{1-3} \\ k_{zx}^{1-1} & k_{zy}^{1-1} & k_{zz}^{1-1} & k_{zx}^{1-2} & k_{zy}^{1-2} & k_{zz}^{1-2} & k_{zx}^{1-3} & k_{zy}^{1-3} & k_{zz}^{1-3} \\ k_{xx}^{2-1} & k_{xy}^{2-1} & k_{xz}^{2-1} & k_{xx}^{2-2} & k_{xy}^{2-2} & k_{xz}^{2-2} & k_{xx}^{2-3} & k_{xy}^{2-3} & k_{xz}^{2-3} \\ k_{yx}^{2-1} & k_{yy}^{2-1} & k_{yz}^{2-1} & k_{yx}^{2-2} & k_{yy}^{2-2} & k_{yz}^{2-2} & k_{yx}^{2-3} & k_{yy}^{2-3} & k_{yz}^{2-3} \\ k_{zx}^{2-1} & k_{zx}^{2-1} & k_{zz}^{2-1} & k_{zx}^{2-2} & k_{zy}^{2-2} & k_{zz}^{2-2} & k_{zx}^{2-3} & k_{zy}^{2-3} & k_{zz}^{2-3} \\ k_{xx}^{3-1} & k_{xy}^{3-1} & k_{xz}^{3-1} & k_{xx}^{3-2} & k_{xy}^{3-2} & k_{xz}^{3-2} & k_{xx}^{3-3} & k_{xy}^{3-3} & k_{xz}^{3-3} \\ k_{yx}^{3-1} & k_{yy}^{3-1} & k_{yz}^{3-1} & k_{yx}^{3-2} & k_{yy}^{3-2} & k_{yz}^{3-2} & k_{yx}^{3-3} & k_{yy}^{3-3} & k_{yz}^{3-3} \\ k_{zx}^{3-1} & k_{zy}^{3-1} & k_{zz}^{3-1} & k_{zx}^{3-2} & k_{zy}^{3-2} & k_{zz}^{3-2} & k_{zx}^{3-3} & k_{zy}^{3-3} & k_{zz}^{3-3} \end{bmatrix}. \quad \text{(S31)}$$

The blue and orange elements are the diagonal components associated with the transverse and longitudinal directions, respectively. The purple elements describe mechanical coupling between degrees of freedom of the same sphere. The green elements describe z-motion coupling between different spheres, whereas the red elements represent the remaining inter-sphere couplings.

The magnitudes of these matrix elements are plotted on a logarithmic scale in Fig. S4d. For the particle radius of 0.1 μm considered here, the longitudinal and transverse diagonal elements differ by a factor of approximately 5. The smaller z-direction elements arise from the relatively weak focusing along z (Fig. S4c). Effective coupling between longitudinal and transverse motion would require coupling terms comparable to this separation between the blue and orange curves. At the particle size used in our study (indicated by the black dashed line in Fig. S4d), however, the

purple and red couplings are far below this scale. Coupling between the transverse and longitudinal directions can therefore be neglected to a good approximation. We may thus restrict the analysis to optical binding along z and use the following force constant matrix:

$$\ddot{\mathbf{K}}_{3D} = \begin{bmatrix} k_{zz}^{1-1} & k_{zz}^{1-2} & k_{zz}^{1-3} \\ k_{zz}^{2-1} & k_{zz}^{2-2} & k_{zz}^{2-3} \\ k_{zz}^{3-1} & k_{zz}^{3-2} & k_{zz}^{3-3} \end{bmatrix}. \tag{S32}$$

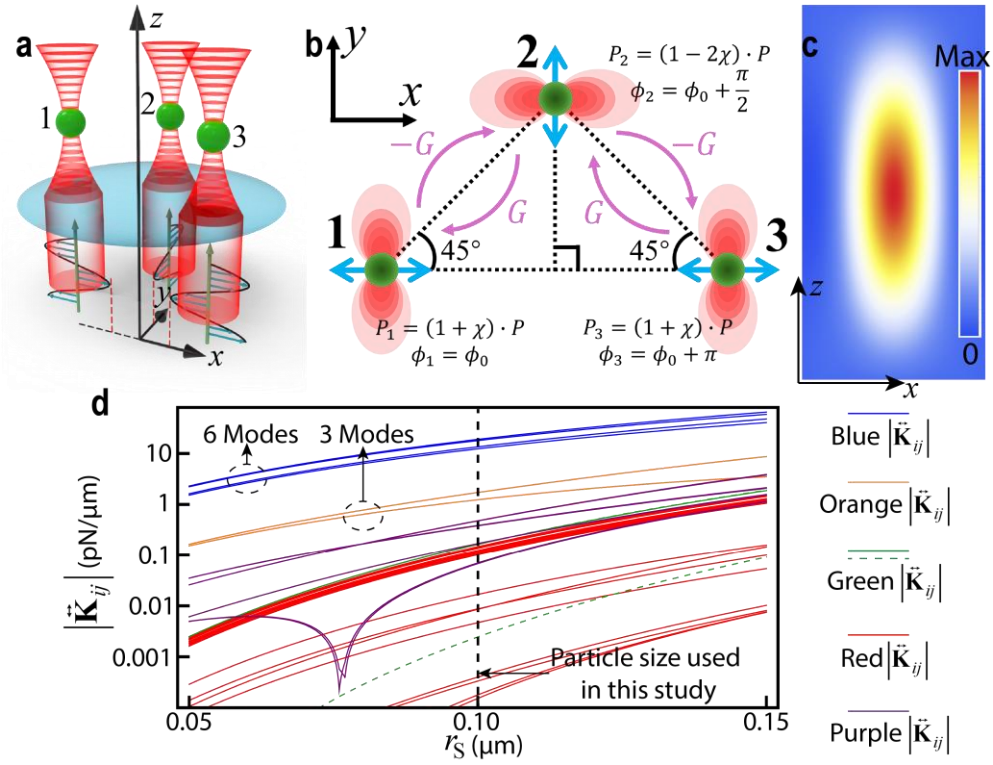

Fig. S4 | Decoupling of the longitudinal and transverse modes. (a) Optical trapping and binding of three silica spheres, each trapped by a linearly polarized beam focused by an objective lens with a numerical aperture of 0.8. (b) Geometry of the incident beams and interparticle coupling. (c) Field-intensity distribution in the xz plane for one focused beam. (d) Magnitudes of the matrix elements corresponding to the transverse trapping stiffness (blue), longitudinal trapping stiffness (orange), and coupling terms (green, red, and purple). The corresponding elements in Eq. (S31) are shown in the same colors.

b) Optimization of the non-Hermitian effects

For the particle radius of 0.1 μm considered here, which is smaller than the wavelength $\lambda = 1.064$ μm, the dipole approximation is expected to be valid. At the separation $d_0 \sim 2.3\lambda$, for which $kd_0 \sim 14$, we retain only singly scattered light because second- and higher-order scattering terms are smaller by at least a factor of order $(kd)^{-1}$. For the polarization configuration in Fig. S4a,b, dipolar particles do not scatter light along the polarization direction; particles 1 and 3 are therefore effectively uncoupled:

$$k_{zz}^{1-3} = k_{zz}^{3-1} \approx 0, \tag{S33}$$

as indicated by the green dashed line in Fig. S4d.

Within the single-scattering approximation, the interactions can be considered pairwise. The scattered-field pattern produces optical-binding coupling between particles 1 and 2 and between particles 2 and 3. For clarity, we first focus on particles 1 and 2 and use a dipole-dipole interaction analysis based on the dyadic Green's function to show how the non-Hermitian coupling arises and how it can be optimized.

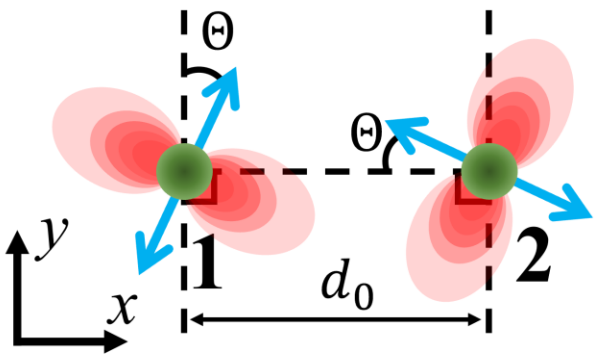

Fig. S5 | Dipole model of two nanoparticles trapped by **orthogonally polarized optical traps in the focal (*xy*) plane.** The optical traps are separated by d_0. Blue double-headed arrows show the trap polarizations, and Θ is the angle between each polarization direction and the corresponding coordinate axis.

In Fig. S5, we choose a coordinate system in which the orthogonal linear polarizations of beams 1 and 2 form an angle Θ with the y and x axes, respectively. Let $\mathbf{r}_i$ denote the position of

sphere *i*, $\mathbf{E}^{i}_{\mathrm{trap}}(\mathbf{r})$ the *i*-th incident trapping field, and $\mathbf{E}^{i\to j}_{\mathrm{sca}}(\mathbf{r})$ the field scattered from sphere *i* to sphere *j*. The total fields incident on sphere *i*, comprising the *i*th trapping field and the field scattered by the other sphere, are

$$\begin{aligned}\mathbf{E}^{1}_{\mathrm{in}}(\mathbf{r}_1) &= \mathbf{E}^{1}_{\mathrm{trap}}(\mathbf{r}_1) + \mathbf{E}^{2\to 1}_{\mathrm{sca}}(\mathbf{r}_1),\\ \mathbf{E}^{2}_{\mathrm{in}}(\mathbf{r}_2) &= \mathbf{E}^{2}_{\mathrm{trap}}(\mathbf{r}_2) + \mathbf{E}^{1\to 2}_{\mathrm{sca}}(\mathbf{r}_2),\end{aligned} \tag{S34}$$

where, within the single-scattering approximation,

$$\begin{aligned}\mathbf{E}^{1\to 2}_{\mathrm{sca}}(\mathbf{r}) &= \ddot{\mathbf{G}}(\mathbf{r}-\mathbf{r}_1)\mathbf{P}_1 \approx \ddot{\mathbf{G}}(\mathbf{r}-\mathbf{r}_1)\alpha\mathbf{E}_{\mathrm{trap}}(\mathbf{r}_1),\\ \mathbf{E}^{2\to 1}_{\mathrm{sca}}(\mathbf{r}) &= \ddot{\mathbf{G}}(\mathbf{r}-\mathbf{r}_2)\mathbf{P}_2 \approx \ddot{\mathbf{G}}(\mathbf{r}-\mathbf{r}_2)\alpha\mathbf{E}_{\mathrm{trap}}(\mathbf{r}_2)\end{aligned} \tag{S35}$$

Here, $\alpha = i6\pi\varepsilon_0 a_1/k^3$ is the electric-dipole polarizability, ε_0 is the vacuum permittivity, $k = 2\pi/\lambda$ is the wavenumber, and a_1 is the first-order Mie coefficient, obtained from the standard expression for $n = 1$ [x]:

$$a_n = \frac{\sigma\psi_n(\sigma k r_{\mathrm{S}})\psi'_n(k r_{\mathrm{S}}) - \psi_n(k r_{\mathrm{S}})\psi'_n(\sigma k r_{\mathrm{S}})}{\sigma\psi_n(\sigma k r_{\mathrm{S}})\xi'_n(k r_{\mathrm{S}}) - \xi_n(k r_{\mathrm{S}})\psi'_n(\sigma k r_{\mathrm{S}})}, \tag{S36}$$

where σ is the relative refractive index, and ψ_n and ξ_n are the Riccati-Bessel functions; primes denote differentiation with respect to the argument. The dyadic Green's function is [xi]

$$\ddot{\mathbf{G}}(\mathbf{R}) = \frac{e^{ikR}}{4\pi\varepsilon_0}\left[\frac{3\mathbf{R}\otimes\mathbf{R} - R^2\ddot{\mathbf{I}}}{R^5}(1-ikR) + k^2\,\frac{R^2\ddot{\mathbf{I}} - \mathbf{R}\otimes\mathbf{R}}{R^3}\right], \tag{S37}$$

where $R = |\mathbf{R}|$, $\otimes$ denotes the Kronecker product, and $\ddot{\mathbf{I}}$ is the identity matrix.

The leading-order, time-averaged ***optical-binding forces*** along *z*, which determine the interparticle couplings, are [xii]:

$$\begin{aligned}F^{1}_{\mathrm{binding}} &\approx \frac{|\alpha|^2}{2}\frac{\partial}{\partial z_1}\mathrm{Re}\left[\mathbf{E}^{*1}_{\mathrm{trap}}(\mathbf{r}_1)\cdot\ddot{\mathbf{G}}(\mathbf{r}_1-\mathbf{r}_2)\mathbf{E}^{2}_{\mathrm{trap}}(\mathbf{r}_2)\right],\\ F^{2}_{\mathrm{binding}} &\approx \frac{|\alpha|^2}{2}\frac{\partial}{\partial z_2}\mathrm{Re}\left[\mathbf{E}^{*2}_{\mathrm{trap}}(\mathbf{r}_2)\cdot\ddot{\mathbf{G}}(\mathbf{r}_2-\mathbf{r}_1)\mathbf{E}^{1}_{\mathrm{trap}}(\mathbf{r}_1)\right].\end{aligned} \tag{S38}$$

At equilibrium, the direct trapping force exerted by each trapping beam vanishes, and terms of order $|\alpha|^3$ are neglected. Although the plane wave incident on the objective has essentially no z-polarized component, focusing generates such a component; on the beam axis, however, the z component of the electric field vanishes. Thus, the on-axis electric fields of trapping beams 1 and 2 can be written, respectively, as [xii]

$$\begin{aligned}\mathbf{E}^1_{\text{trap}}(z_1) &= E_{\text{trap}}(z_1)\left(\sin\Theta, \cos\Theta, 0\right),\\ \mathbf{E}^2_{\text{trap}}(z_2) &= E_{\text{trap}}(z_2)\left(-\cos\Theta, \sin\Theta, 0\right),\end{aligned} \tag{S39}$$

where Θ specifies the polarization, as shown in Fig. S5. Near the focal plane, the incident-field magnitude can be approximated as [xii]

$$E_{\text{trap}}(z_i) \approx \sqrt{\frac{4P_i}{\pi c \varepsilon_0 \omega_0^2}} \exp\left[i\left(k - \frac{1}{z_R} \right) z_i + i\phi_i \right] \tag{S40}$$

where P_i is the power of beam i, c is the speed of light in vacuum, ω_0 is the beam waist, z_R is the Rayleigh range, and ϕ_i is the optical phase at the focal plane.

In the far-field regime, where the interparticle distance d_0 is much greater than $1/k$, the dominant contribution to the dyadic Green's function scales as $1/R$. The z component of the optical-binding force can therefore be approximated as

$$F^i_{\text{binding},z} \approx \frac{C}{kd_0} \sin\left(2\Theta\right)\left[\cos\left(kd_0\right)\cos\left(\Delta\phi_0\right) \mp \sin\left(kd_0\right)\sin\left(\Delta\phi_0\right) \right]\left(\mp z_1 \pm z_2 \right)\hat{\mathbf{e}}_z, \tag{S41}$$

where $C = \dfrac{|\alpha|^2 k^3 \left(k - \dfrac{1}{z_R} \right)^2 \sqrt{P_1 P_2}}{4\pi^2 c \varepsilon_0^2 \omega_0^2}$, $\Delta\phi_0 = \phi_2 - \phi_1$ is the initial phase difference between the two traps, z_i is the z coordinate of particle i, and $\hat{\mathbf{e}}_z$ is the unit vector along z. From Eq. (S41), the corresponding contributions to the trapping stiffness and the coupling terms of the force constant matrix are

$$\begin{cases} \dfrac{\partial F^1_{\text{binding},z}}{z_1} = -(D-G), & \dfrac{\partial F^1_{\text{binding},z}}{z_2} = (D-G), \\ \dfrac{\partial F^2_{\text{binding},z}}{z_1} = (D+G), & \dfrac{\partial F^2_{\text{binding},z}}{z_2} = -(D+G), \end{cases}, \tag{S42}$$

Here, $D = \dfrac{C\sin(2\Theta)}{kd_0}\cos(kd_0)\cos(\Delta\phi_0)$ and $G = \dfrac{C\sin(2\Theta)}{kd_0}\sin(kd_0)\sin(\Delta\phi_0)$ are the symmetric and antisymmetric coupling terms, respectively. The magnitudes of D and G can be tuned through the polarization angle Θ. The interparticle distance d_0 and phase difference $\Delta\phi_0$ further control the relative symmetric and antisymmetric contributions in this dipole-dipole interaction model. To maximize the non-Hermitian (antisymmetric) coupling, we choose d_0 and $\Delta\phi_0$ such that $D = 0$. Equation (S42) then reduces to

$$\begin{cases} \dfrac{\partial F^1_{\text{binding},z}}{z_1} = G, & \dfrac{\partial F^1_{\text{binding},z}}{z_2} = -G, \\ \dfrac{\partial F^2_{\text{binding},z}}{z_1} = G, & \dfrac{\partial F^2_{\text{binding},z}}{z_2} = -G, \end{cases}. \tag{S43}$$

Similarly, the interaction between spheres 2 and 3 gives

$$\begin{cases} \dfrac{\partial F^{2\Diamond}_{\text{binding},z}}{z_2} = G, & \dfrac{\partial F^2_{\text{binding},z}}{z_3} = -G, \\ \dfrac{\partial F^3_{\text{binding},z}}{z_2} = G, & \dfrac{\partial F^3_{\text{binding},z}}{z_3} = -G, \end{cases}, \tag{S44}$$

Here, $\Diamond$ denotes the contribution of the term $\dfrac{\partial F^{2\Diamond}_{\text{binding},z}}{z_2}$ from the interaction between spheres 2 and 3, just to distinguish from the contribution from the interaction between sphere 1 and 2. This contribution is exactly opposite to that from the interaction between spheres 1 and 2, denoted by $\dfrac{\partial F^2_{\text{binding},z}}{z_2}$ in Eq. (S43).

The power and phase of each focused beam are shown in Fig. S4b, where $P_1 = P_3 = (1+\chi)P$ and $P_2 = (1-2\chi)P$. The separations between particles 1 and 2 and between

particles 2 and 3 are both approximately 2.44 μm (2.3λ). We further assume that, when $\chi = 0$, all three particles have the same vibrational frequency Ω_0 along z in the absence of optical-binding forces. Applying the conditions in Eqs. (S33), Eq. (S32) becomes

$$\ddot{\mathbf{K}}_{3D} = \begin{bmatrix} k_{11} & -G & 0 \\ G & k_{22} & -G \\ 0 & G & k_{33} \end{bmatrix} = \begin{bmatrix} -m(1+\chi)\Omega_0^2 - G(\chi) & -G(\chi) & 0 \\ G(\chi) & -m(1-2\chi)\Omega_0^2 & -G(\chi) \\ 0 & G(\chi) & -m(1+\chi)\Omega_0^2 + G(\chi) \end{bmatrix}, \tag{S45}$$

with $G(\chi) \propto \sqrt{(1-2\chi)(1+\chi)}$. In the main text, χ ranges from -0.3 to 0, while $\sqrt{(1-2\chi)(1+\chi)}$ varies correspondingly from 1.06 to 1. We may therefore treat $G(\chi)$ as approximately constant. The contribution $\frac{\partial F^2_{\text{binding},z}}{z_2} = -G$ in Eq. (S43) is exactly cancelled by $\frac{\partial F^{2\Diamond}_{\text{binding},z}}{z_2} = G$ in Eq. (S44).

Supplementary Note 4: Measurement of the imaginary components of the vibrational frequencies.

For particles optically trapped or bound in a medium of finite viscosity, the vibrational frequencies obtained from the equations of motion contain both real and imaginary components, as shown in Eq. (S7). Experimentally measured particle trajectories yield the power spectral density (PSD), from whose peaks the real frequencies can be extracted (Fig. S6).

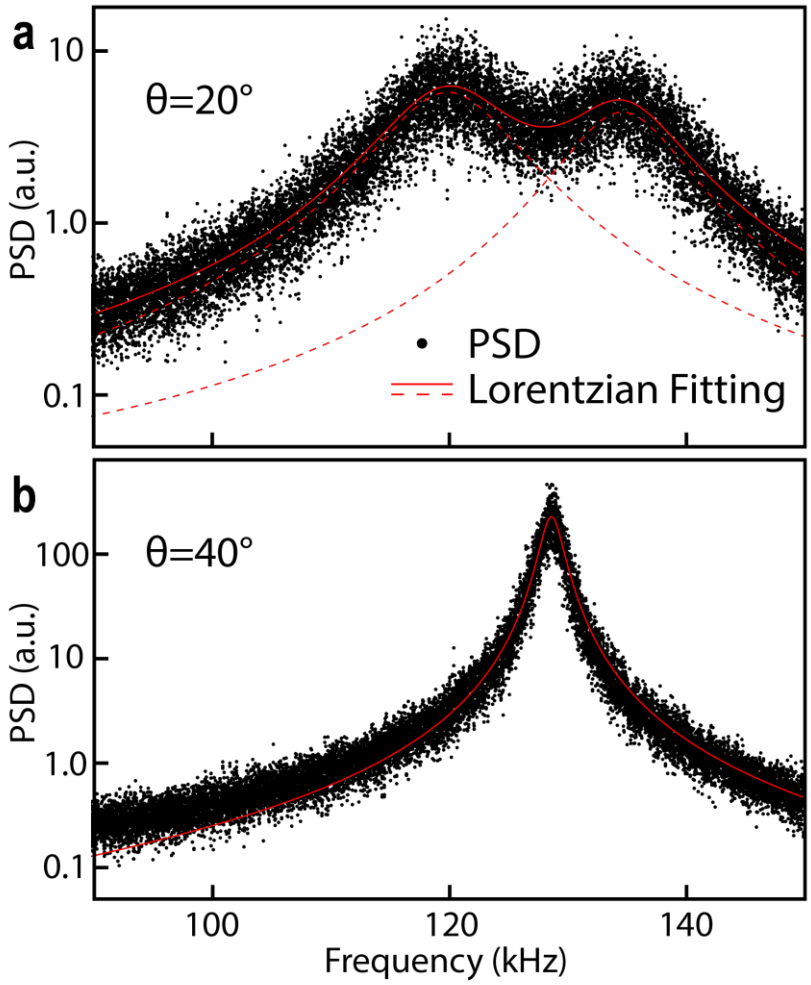

Fig. S6 | Extraction of imaginary frequencies by Lorentzian fitting for a single optically trapped particle. (a) PSD and corresponding Lorentzian fits before **the** EP ($\theta = 20°$). (b) PSD and corresponding Lorentzian fits after **the** EP ($\theta = 40°$).

The imaginary component originates from background damping and may also arise when K_i is complex. Experimentally, it can be obtained from the correlation between, for example, $x(t)$ and $y(t)$ motions [xiii]:

$$\langle x(t+\tau)y(t)\rangle \propto e^{\mathrm{Im}\left[\Omega_i^{\pm}\right]\tau}. \tag{S46}$$

Before the exceptional point, $\mathrm{Im}\left[\Omega_i^{\pm}\right]=-\frac{\gamma}{2m}$ contains only the contribution from background damping. After the exceptional point, $\mathrm{Im}\left[\Omega_i^{\pm}\right]$ also contains the contribution from the complex K_i.

The imaginary frequency can also be obtained by Lorentzian fitting (Fig. S6a,b), with the half-width at half-maximum giving its value. The imaginary frequencies determined by the correlation analysis and Lorentzian fitting agree, as shown in Fig. S7.

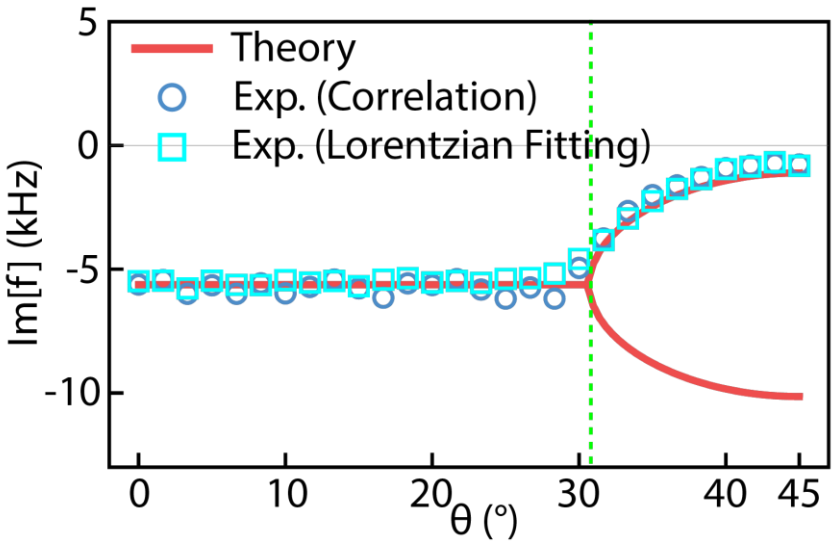

Fig. S7 | Comparison of two methods for measuring the imaginary frequencies of a single optically trapped **particle.** The red line is the theoretical prediction. Blue circles show experimental results from motion-correlation analysis, and cyan squares show those from Lorentzian fitting.

Supplementary Note 5: Neutralization of the net charges on optically bound particles.

After the three particles were trapped and the vacuum chamber was pumped down to the required pressure, each particle initially carried tens to hundreds of elementary charges [xiv]. The resulting electrostatic interactions produced mechanical coupling between the particles. The electrostatic coupling rate g_e between two charged particles is [xv]:

$$g_e = \frac{q_1 q_2}{8\pi\varepsilon_0 m\omega'^2 d_0^3} \tag{S47}$$

where q_1 and q_2 are the charges on the two particles, ε_0 is the vacuum permittivity, m is the particle mass, and d_0 is the interparticle distance. The modified frequency ω' is defined as $\omega' = \sqrt{\omega^2 - \frac{q_1 q_2}{4\pi\varepsilon_0 m d_0^3}}$. As d_0 decreases, the electrostatic coupling rate increases approximately as d_0^{-3} and can become comparable to the optical coupling rate at small separations.

To isolate the light-induced dipole-dipole interactions, we therefore simultaneously neutralized the three particles, thereby eliminating electrostatic interactions within the system. High-voltage discharges generated a plasma containing positive and negative ions, which changed the net charge on each particle. Meanwhile, two needle electrodes mounted on a three-dimensional piezo stage and aligned along the *x* axis applied an electric drive to the particles. The motion signals of the charged particles were sent to lock-in amplifiers (MFLI, Zurich Instruments), which demodulated the oscillation amplitude and phase within a narrow frequency band centred on the drive frequency. This procedure enabled real-time monitoring and neutralization of the particle charges. Figure S8 shows the simultaneous charge-control process. The amplitude is proportional to the magnitude of the charge, whereas the phase encodes its polarity. After repeated high-voltage discharges, all three particles were simultaneously neutralized.

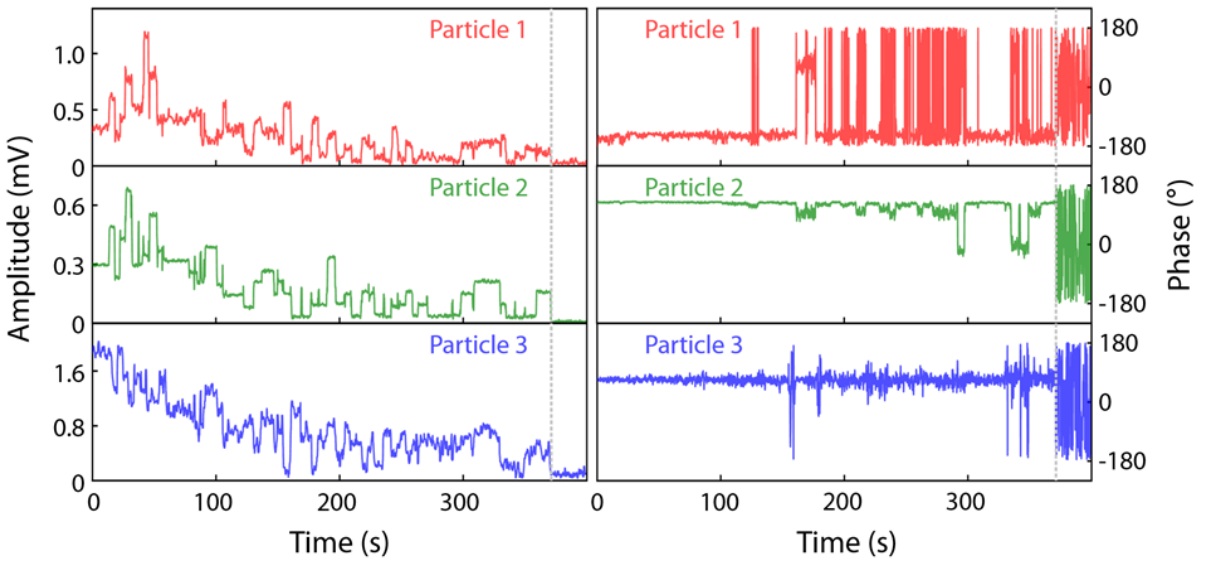

Fig. S8 | Simultaneous control of **the net charges o**n **particle 1 (red), particle 2 (green)**, **and particle 3 (blue).** Amplitude and phase are demodulated from the particles' *x*-motion signals within a narrow frequency band of the applied electric drive. Step-like amplitude changes indicate discrete changes in particle charge, whereas the phase indicates charge polarity. For charge-neutral particles, the phase becomes random. The grey dashed line marks the point at which all three particles are simultaneously neutralized.

Supplementary Note 6: Fluctuation theorem for non-Hermitian optical trapping and binding systems.

Figure 4 of the main text shows real and virtual vortices in the optical trapping system (see also Fig. S9a,b) and optical binding system (see also Fig. S9c,d), respectively. These vortices, generated by non-Hermitian force fields, bias particle motion in a preferred direction, although reverse trajectories remain possible. The ratio of the forward and reverse probabilities obeys

$$\frac{P(W)}{P(-W)} = e^{W/k_{\mathrm{B}}T} \tag{S48}$$

where $P(W)$ is the probability of observing work W in the forward protocol, $P(-W)$ is the probability of observing work $-W$ in the reverse protocol, k_{B} is the Boltzmann constant, and T is the temperature of the background medium. Equation (S48) is the Crooks fluctuation theorem. It provides a statistical description of systems far from equilibrium and relates forward and reverse probabilities to entropy production and dissipation. Within the linear approximation, the work is

$$W = \oint_C \mathbf{F} \cdot d\mathbf{l} = 2g\pi r_C^2 = 2gA_C \tag{S49}$$

for a particle moving around an assumed circular loop C. Here, r_C and A_C are the radius and area of the loop, respectively, and g is the antisymmetric component of the force constant matrix that characterizes the nonconservative force. In Fig. S9e,f, we report the ensemble-averaged r_C ($\sqrt{\langle r^2 \rangle}$) for optical trapping and binding, respectively. The results show that r_C increases with the degree of non-Hermiticity. The corresponding increase in W therefore produces the larger probability ratio described by Eq. (S49).

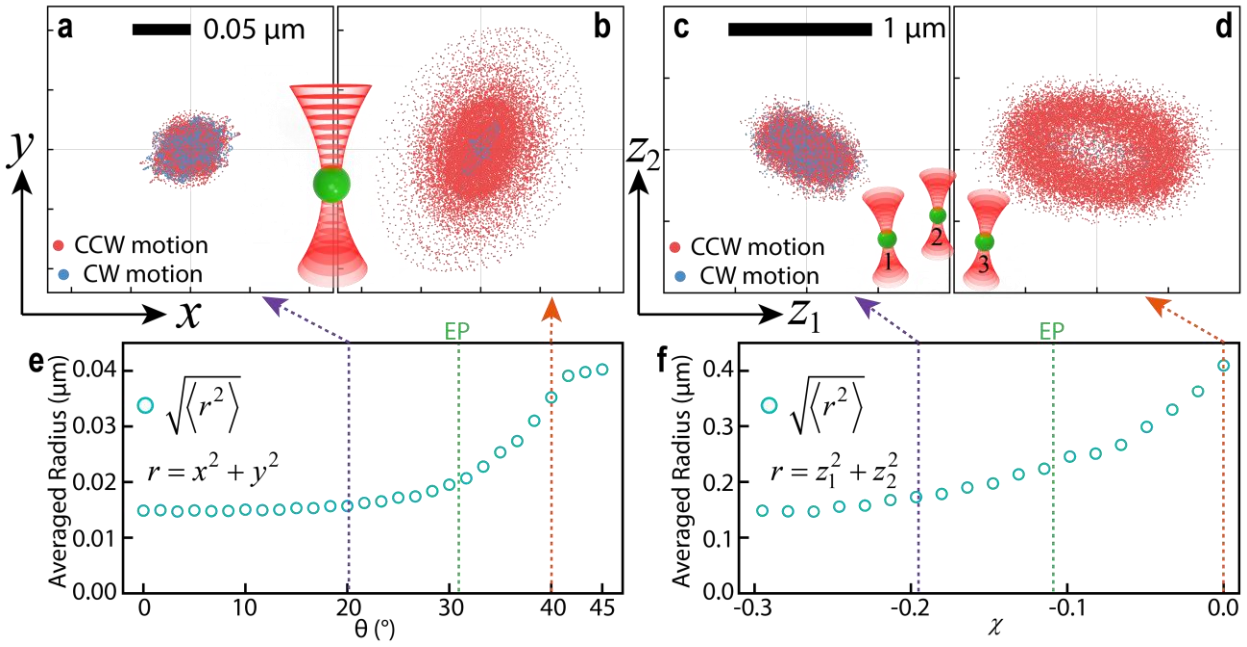

Fig. S9 | Mean trajectory radius as a function of non-Hermiticity. Trajectories for optical trapping (a,b) and optical binding (c,d), together with the corresponding mean radii (e,f).

References

i Gordon, R., Kawano, M. & Blakely, J. T. Optohydrodynamic theory of particles in a dual-beam optical trap. *Phys. Rev. B* **77**, 245125 (2008).

ii Ng, J. Lin, Z. F., Chan, C. T. & Sheng, P. Photonic clusters formed by dielectric microspheres: Numerical simulations. *Phys. Rev. B* **72**, 085130 (2005).

iii Gieseler, J., Deutsch, B., Quidant, R. & Novotny, L. Subkelvin Parametric Feedback Cooling of a Laser-Trapped Nanoparticle. *Phys. Rev. Lett.* **109**, 103603 (2012).

iv Seyranian, A. P. & Mailybaev, A. A. Multiparameter stability theory with mechanical applications. *World Scientific* (2003).

v Tisseur, F., & Meerbergen, K. The quadratic eigenvalue problem. *SIAM review*, **43**(2), 235-286 (2001).

vi Tisseur, F., & Meerbergen, K. The quadratic eigenvalue problem. *SIAM review*, **43**(2), 235-286 (2001).

vii Ng, J., Lin, Z., & Chan, C. T. Theory of optical trapping by an optical vortex beam. *Phys. Rev. Lett.*, **104**(10), 103601 (2010).

viii Nieminen, T. A., Stilgoe, A. B., Heckenberg, N. R. & Rubinsztein-Dunlop, H. Angular momentum of a strongly focused Gaussian beam. *J. Opt. A: Pure Appl. Opt.* **10**, 115005 (2008).

ix Nieminen, T. A., Stilgoe, A. B., Heckenberg, N. R. & Rubinsztein-Dunlop, H. Angular momentum of a strongly focused Gaussian beam. *J. Opt. A: Pure Appl. Opt.* **10**, 115005 (2008).

x Xu, Y. L., & Gustafson, B. Å. A generalized multiparticle Mie-solution: further experimental verification. *Journal of Quantitative Spectroscopy and Radiative Transfer*, 70(4-6), 395-419. (2001).

xi Jackson, J. D., & Fox, R. F. Classical electrodynamics (1999).

xii Yokomizo, K. & Ashida, Y. Non-Hermitian physics of levitated nanoparticle array. *Phys. Rev. Res.* **5**, 033217 (2023).

xiii Liška, V. *et al.* PT-like phase transition and limit cycle oscillations in non-reciprocally coupled optomechanical oscillators levitated in vacuum. *Nat. Phys.* **20**, 1622–1628 (2024).

xiv Zhu, S. *et al.* Nanoscale electric field sensing using a levitated nano-resonator with net charge. *Photon. Res., PRJ* **11**, 279–289 (2023).

xv Rieser, J. *et al.* Tunable light-induced dipole-dipole interaction between optically levitated nanoparticles. *Science* **377**, 987–990 (2022).